Langmuir

Article

pubs.acs.org/Langmuir

Surface Shear Rheology of Adsorption Layers from the Protein HFBII Hydrophobin: Effect of Added β-Casein

Gergana M. Radulova,[†] Konstantin Golemanov,[†,‡] Krassimir D. Danov,[†] Peter A. Kralchevsky,*[,†] Simeon D. Stoyanov,[‡] Luben N. Arnaudov,[‡] Theodorus B. J. Blijdenstein,[‡] Eddie G. Pelan,[‡] and Alex Lips[§]

[†]Department of Chemical Engineering, Faculty of Chemistry, Sofia University, 1164 Sofia, Bulgaria

[‡]Unilever Research & Development, 3133AT Vlaardingen, The Netherlands

[§]Unilever Research & Development, Port Sunlight, Wirral, Merseyside CH63 3JW, U.K.

Supporting Information

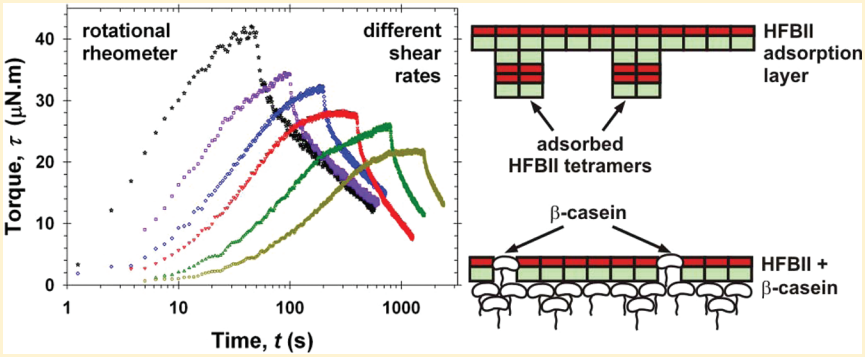

ABSTRACT: The surface shear rheology of hydrophobin HFBII adsorption layers is studied in angle-ramp/relaxation regime by means of a rotational rheometer. The behavior of the system is investigated at different shear rates and concentrations of added β-casein. In angle-ramp regime, the experimental data comply with the Maxwell model of viscoelastic behavior. From the fits of the rheological curves with this model, the surface shear elasticity and viscosity, E_{sh} and η_{sh}, are determined at various fixed shear rates. The dependence of η_{sh} on the rate of strain obeys the Herschel−Bulkley law. The data indicate an increasing fluidization (softening) of the layers with the rise of the shear rate. The addition of β-casein leads to more rigid adsorption layers, which exhibit a tendency of faster fluidization at increasing shear rates. In relaxation regime, the system obeys a modified Andrade's (cubic root) law, with two characteristic relaxation times. The fact that the data comply with the Maxwell model in angle-ramp regime, but follow the modified Andrade's low in relaxation regime, can be explained by the different processes occurring in the viscoelastic protein adsorption layer in these two regimes: breakage and restoration of intermolecular bonds at angle-ramp vs solidification of the layer at relaxation.

1. INTRODUCTION

The interfacial rheology of protein adsorption layers has been a subject of intensive studies in relation to the properties of protein-stabilized emulsions,[1−6] foams,[7−9] and mixed systems such as lipids + proteins[10,11] and surfactants + proteins.[12−17] Detailed information on the investigated systems, experimental techniques, and theoretical models can be found in review articles on interfacial shear rheology.[17−22]

The subject of the present study is the rheological behavior of adsorption layers from the protein HFBII hydrophobin at the air−water interface. The most remarkable property of the HFBII layers is that they solidify soon after their formation and that their surface shear elastic and viscous moduli are considerably higher than those for other proteins.[9] Bubbles formed in HFBII solutions preserve the irregular (nonspherical) shape they have had at the moment of solidification of their surfaces.[23] Foams composed of such bubbles exhibit an exceptional stability.[8] This is related to the fact that the solidification of the adsorption layers at the bubble surfaces suppresses the foam disproportionation. From a mechanical viewpoint, the indicator for solidification is the surface *shear* elasticity, E_{sh}, which is zero for fluid interfaces but has nonzero values for solidified (elastic or viscoelastic) adsorption layers. Comprehensive information on the properties of hydrophobins and their applications can be found in recent publications.[23−33]

In general, the surface shear elasticity is due to the formation of lateral bonds between the adsorbed molecules. For a medium with viscoelastic behavior, the interfacial shearing leads to breakage and restoration of such bonds. However, a prolonged and intensive shearing may reduce E_{sh} and cause softening, and even fluidization, of the protein adsorption layer. After ceasing the external mechanical impact, the layer solidifies again and the

Received: December 27, 2011
Revised: February 7, 2012
Published: February 9, 2012

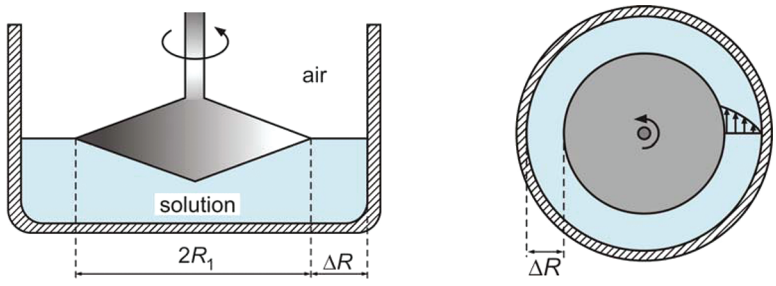

Figure 1. Sketch of the used rotational rheometer with biconical tool: (a) vertical cross-section and (b) top view. The dimensions are R_1 = 2.81 cm and $\Delta R = R_2 - R_1$ = 0.19 cm.

interfacial stresses might relax completely or incompletely.[34−36] The process of relaxation (solidification) and its characteristic time are important for the longevity of protein-stabilized foams and emulsions.

In the present article, we report results from the investigation of the shear rheology of HFBII adsorption layers at the air−water interface by means of a rotational rheometer in angle-ramp/relaxation regime. To minimize the external impact on the surface viscoelastic properties, the angle-ramp is carried out at the smallest shear rates that are achievable with the used apparatus. Adopting an adequate rheological model, from the obtained data we determine the surface shear elasticity and viscosity of the HFBII adsorption layers. In addition, from the data obtained in the relaxation regime, the characteristic time of surface solidification is determined. The effects of the shearing time and rate, as well as of added β-casein, on the rheological behavior are investigated. The results obtained in angle-ramp/relaxation regime will be compared with results obtained in oscillatory regime in a subsequent study.

2. MATERIALS AND METHODS

In our experiments, the protein HFBII was used, which is a class II hydrophobin isolated from the fungus *Trichoderma reesei* following the procedure described in ref 23. A stock solution of concentration 0.1 wt % HFBII was prepared. Before each experiment, the stock solution was sonicated in an ultrasonic bath for 5 min to break up the protein aggregates and then it was diluted to 0.005 wt %. Just before its loading in the rheometer, the diluted solution was also sonicated, to break up newly formed aggregates. All experiments were performed at a temperature of 25 °C.

The used β-casein was supplied by Sigma (β-casein from bovine milk, minimum 90%, cat. No: C6905). The mixed solutions of β-casein and HFBII were prepared with 0.005 wt % HFBII at different β-casein concentrations ranging from 0.015 to 0.135 wt %. Taking into account the molecular weight of β-casein (24 000 g/mol) and that of HFBII (7200 g/mol), the molar ratio β-casein/HFBII in the used solutions ranged from 0.9 to 8.1.

For each solution, the experiment was repeated at least three times. Before each run, the solution in the experimental cell was replaced with a newly prepared solution. After its loading, we waited for 5 min before the start of the rheological measurements. This period of time is needed for the formation and consolidation of the adsorption layer. In general, the rheological properties of the protein adsorption layers vary with the surface age.[2,4,12,14,37,38] For this reason, in our experiments the aging time was the same, 5 min in all runs. Similar aging time has been used by other authors.[4]

The measurements were carried out with a rotational rheometer Bohlin Gemini, Malvern UK. This rheometer is equipped with a biconical tool (see Figure 1) for interfacial shear rheology measurements. The biconical tool is placed in a working cell, where the investigated solution is poured up to the edge of the tool. The outer radius of the bicone is R_1 = 2.81 cm; the inner radius of the wall of the cylindrical cell is R_2 = 3.0 cm, and the distance between them is ΔR = 0.19 cm. The latter represents the width of the ring-shaped HFBII adsorption monolayer that is subjected to shear deformation.

In angle-ramp/relaxation regime, the rotation angle θ increases with a constant speed $\dot{\theta} \equiv d\theta/dt$, and afterward, θ is kept constant ($\dot{\theta} \equiv 0$) and the torque τ relaxes. During the whole experiment, θ and τ were recorded as functions of time t. This regime is one of the operation modes of this class of rheometers,[39] but to the best of our knowledge, it has not been applied for investigating the rheology of protein adsorption layers so far.

To protect the elastic protein adsorption layer against disruption, we carried out the experiments at very low angular velocities ($0.009 \leq \dot{\theta} \leq 0.28$ mrad/s), which are at the lower limit of velocities achievable by the used apparatus. The test measurements at the surface of pure water give $\tau = 0$ for $\dot{\theta} \leq 0.28$ mrad/s, i.e. there is no rheological response (or it is below the accuracy threshold of the used apparatus). This is not surprising, because the aqueous phase is a viscous fluid whose rheological response is proportional to the velocity and is extremely low at the low velocities used in our experiments. In contrast, the elastic response of the hydrophobin adsorption layer is proportional to θ (rather than to $\dot{\theta}$), so that its rheological response is registered with a good accuracy by the apparatus (see below). In other words, the measured torque is completely due to the viscoelastic adsorption layer, and it is experimentally confirmed that the viscous friction with the subphase is completely negligible at the used very low rotation rates.

3. EXPERIMENTAL RESULTS AND DISCUSSION

3.1. Effect of the Shearing Time. The typical behavior of the investigated systems in angle-ramp/relaxation regime is shown in Figure 2 for 0.005 wt % HFBII solutions. The torque τ increases with the increase of the rotation angle θ, and afterward, τ relaxes at fixed θ. The values of θ and t, which correspond to the end of the angle ramp (and the beginning of relaxation), are denoted by θ_b and t_b. In Figure 2, we compare three rheological curves obtained at three different values of the rotation (shearing) time, t_b = 200, 400, and 800 s, all other conditions being the same. For the experimental (relatively low) shear rate, $\dot{\theta}$ = 35 μrad/s, the rheological behavior of the HFBII layers is insensitive to t_b for $t < t_b$. In relaxation regime ($t > t_b$), it seems that the three curves in Figure 2 have different behavior, but in fact they correspond to the same characteristic relaxation time; see section 5.1 below.

For the measurements with hydrophobin layers in angle-ramp/relaxation regime, it is typical that if one experiment is repeated many times, the reproducibility of the obtained τ-vs-t curves is not perfect. Most of the experimental curves obtained under identical conditions are close to each other, but there are also curves that markedly deviate from the other ones.

dx.doi.org/10.1021/la205113w | *Langmuir* 2012, 28, 4168−4177

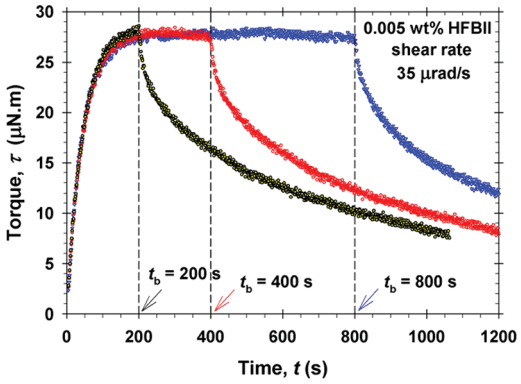

Figure 2. Experimental curves obtained in angle-ramp/relaxation regime: plots of the torque, τ, vs time, t, for aqueous solutions of 0.005 wt % HFBII at the same shear rate, $\dot{\theta} = 35$ μrad/s at $t < t_b$, but at three different shearing times: t_b = 200, 400, and 800 s. The relaxation of τ happens at a fixed rotation angle: $\dot{\theta} = 0$ at $t > t_b$.

Possible sources of irreproducibility are the aggregation in the HFBII solutions and the formation of a stiff adsorption layer with many voids[27,40,41] (the area fraction and size-distribution of the voids are irreproducible). Another source of irreproducibility can be the attachment of HFBII aggregates to the adsorption layer[23,24,27,42,43] and the formation of local multilayered spots on the interface. Here, we present only experimental curves that exhibit repeating behavior, whereas the curves with anomalous behavior have been ignored.

3.2. Effect of the Shearing Rate. Figures 3 and 4 show experimental results for the torque, τ, vs time, t, at different values of the angular velocity, $\dot{\theta}$. The two investigated systems are solutions of HFBII (Figure 3) and HFBII + β-casein (Figure 4). The reproducibility of the experiments was higher for the solutions with HFBII alone and lower for the solutions of HFBII + β-casein. The six curves in each figure correspond to six different fixed values of $\dot{\theta}$, which vary from 8.73 to 280 μrad/s. For each of the two systems, the greater shearing rate, $\dot{\theta}$, leads to a greater value of the measured torque, τ. For all $\dot{\theta}$, the angle-ramp regime ends at the same rotation angle $\theta = \theta_b$ = 14 mrad and after that the adsorption layer relaxes at $\dot{\theta} = 0$. At the lowest angular velocity $\dot{\theta}$, the shearing time is $t_b = \theta_b/\dot{\theta}$ = 1604 s, whereas at the highest $\dot{\theta}$ the shearing time is only t_b = 50 s. Because of this difference, the data in Figures 3a and 4a are shown in logarithmic scale along the horizontal axis to visualize the rheological response of the adsorption layer at the early times ($t < t_b$). In addition, to compare the experimental curves at intermediate and long times ($t \geq t_b$), the data for τ are plotted vs the dimensionless time t/t_b in Figures 3b and 4b. The latter plots visualize also the dependence of the torque, τ, on the rotation angle, θ, insofar as in angle-ramp regime $t/t_b = \theta/\theta_b$, and θ_b is the same for all runs in Figures 3 and 4. These figures present the basic set of data for testing different rheological models in sections 4 and 5.

At the higher angular velocities, some of the experimental curves exhibit small undulations, which are better visible in Figure 3b. They are due to the action of the mechano-electronic feedback built in the apparatus, which keeps constant the rotation velocity in angle-ramp regime.

3.3. Effect of Added β-Casein. Figure 5 shows the effect of added β-casein on the HFBII adsorption layers. On the one hand, for 0.1 wt % β-casein solution (without HFBII), the measured torque is so low, that it cannot be registered by the used apparatus; see the horizontal experimental curve at the bottom of Figure 5. On the other hand, if HFBII is present the effect of β-casein on the measured shear stress is relatively weak. Hence, despite the presence of β-casein, HFBII forms elastic layer at the air/water interface. Note that in this series of experiments, the β-casein weight concentration is up to 27 times greater that of HFBII. Under such conditions, the weak effect of β-casein (Figure 5) indicates (i) greater surface activity of HFBII and (ii) weak interaction between HFBII and β-casein. Indeed, in the opposite case of strong adhesive interaction between the two proteins, most of the HFBII molecules would be incorporated in joint aggregates with β-casein in the bulk, so that HFBII would not be able to form a dense adsorption layer, which contradicts the experimental results. A further discussion of the data in Figure 5 can be found in section 4.3.

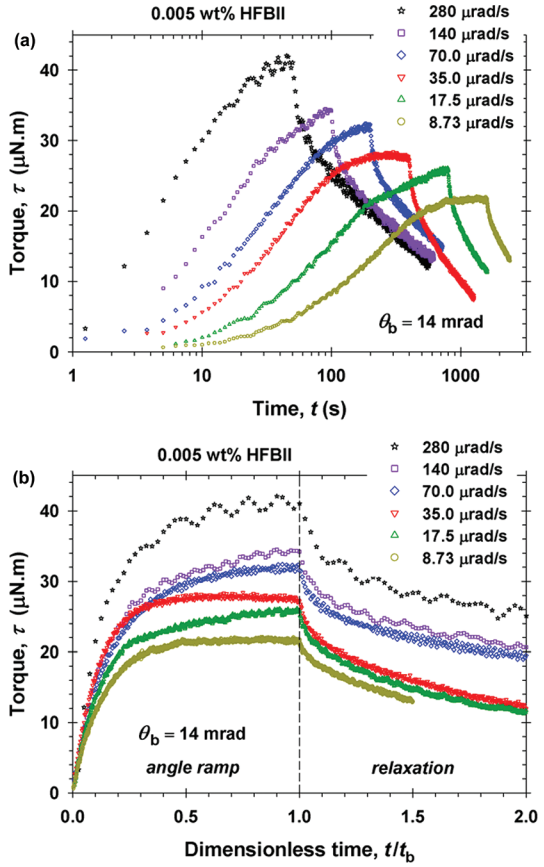

Figure 3. Data for adsorption layers from 0.005 wt % HFBII solutions. (a) Plot of the torque τ vs time t at six different angular velocities, $\dot{\theta}$, denoted in the figure. For all curves, the angle ramp ends at the same rotation angle $\theta = \theta_b$ = 14 mrad, and after that the adsorption layer relaxes at $\dot{\theta} = 0$. (b) The same data are plotted vs t/t_b, where the time moment $t_b \equiv \theta_b/\dot{\theta}$ corresponds to the boundary between the angle-ramp and relaxation regimes.

4. ANGLE-RAMP REGIME: DATA INTERPRETATION

4.1. Comparison with the Maxwell Model. In angle-ramp regime, at the early times ($t \ll t_b$), we do not observe indications for the existence of yield-stress effects. The shapes of the experimental curves in Figures 2−5 look like the curves predicted by the Maxwell model; see Figure 6. (In angle-ramp regime, the alternative Kelvin model predicts a linear increase of τ with time, which is inconsistent with the experimental results.) In the Maxwell model, the total strain, θ, is equal to the

dx.doi.org/10.1021/la205113w | Langmuir 2012, 28, 4168−4177

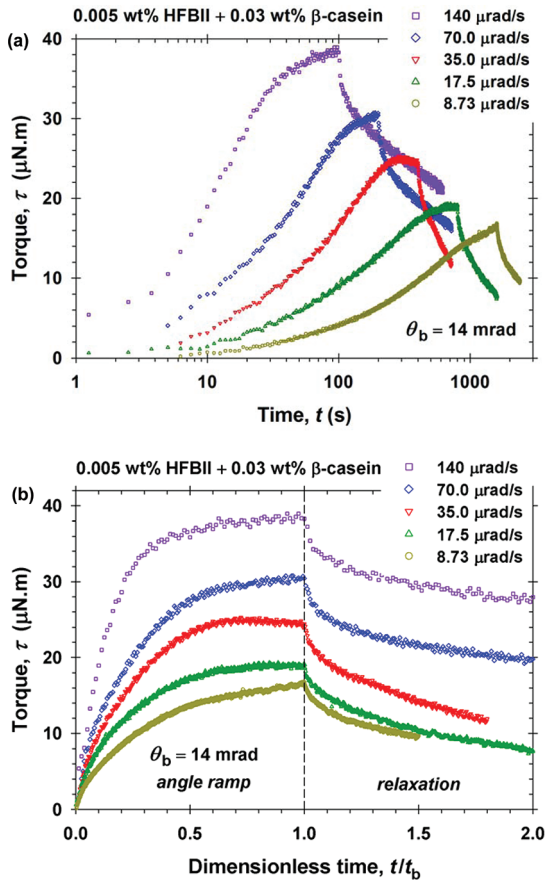

Figure 4. Data for adsorption layers from 0.005 wt % HFBII + 0.03 wt % β–casein. (a) Plot of the torque τ vs time t at five different angular velocities, $\dot{\theta}$, denoted in the figure. (b) The same data are plotted vs t/t_b, where the time moment $t_b \equiv \theta_b/\dot{\theta}$ corresponds to the boundary between the angle-ramp and relaxation regimes, at which $\theta = \theta_b = 14$ mrad for all runs.

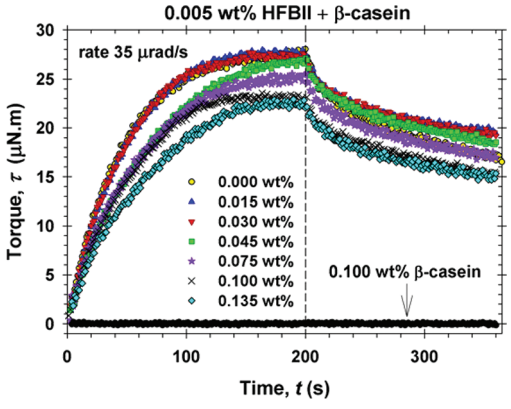

Figure 5. Effect of added β-casein on the torque, τ, vs time, t, rheological curves in angle-ramp/relaxation regime at 0.005 wt % HFBII; shearing time t_b = 200 s; shear rate $\dot{\theta}$ = 35 μrad/s, and at different concentrations of β-casein denoted in the figure.

sum of the deformations of the elastic and viscous elements. In terms of rates-of-strain, this relationship reads as follows:

$$\frac{1}{G}\frac{d\tau}{dt} + \frac{\tau}{\eta} = \dot{\theta} \tag{1}$$

where G and η are, respectively, elastic and viscous coefficients. In the conventional Maxwell model, G and η are independent

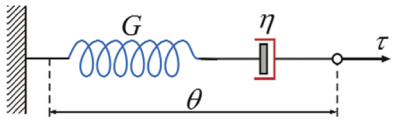

Figure 6. Sketch of the Maxwell model of a viscoelastic body: consecutively connected elastic element (spring) of modulus G and viscous element (dash-pot) characterized by a viscous coefficient η. The stress, τ, acting on the two elements is the same, whereas the total strain, θ, equals the sum of the strains of the two elements.

of time, t. Moreover, in the angle-ramp regime the shear rate $\dot{\theta}$ is also independent of t. Then, the integration of eq 1 gives the following:

$$\tau = \eta\dot{\theta}\left[1 - \exp\left(-\frac{G}{\eta}t\right)\right] \tag{2}$$

In the angle-ramp regime, $t = \theta/\dot{\theta}$, so that eq 2 can be expressed also in the form:

$$\tau = \eta\dot{\theta}\left[1 - \exp\left(-\frac{G\theta}{\eta\dot{\theta}}\right)\right] \tag{3}$$

At each fixed angular velocity $\dot{\theta}$, the experimental τ-vs-θ curve excellently agrees with eq 3 (see the regression coefficients in Table 1). The fits are illustrated in Figure 7, for the two

Table 1. Parameters of the Maxwell Model Determined from the Fits of the Data in Angle-Ramp Regime, $t < t_b$ (Figures 3 and 4)

$\dot{\theta}$ (μrad/s)	E_{sh} (mN/m)	η_{sh} (N·s/m)	regr coeff
0.005 wt % HFBII			
8.73	142 ± 5	30.7 ± 0.9	0.9991
17.5	187 ± 8	19.9 ± 0.6	0.9990
35	224 ± 8	9.8 ± 0.4	0.9987
70	153 ± 6	5.6 ± 0.3	0.9985
140	158 ± 6	3.0 ± 0.1	0.9970
280	248 ± 8	1.8 ± 0.1	0.9917
0.005 wt % HFBII + 0.03 wt % β-casein			
8.73	46 ± 3	24.1 ± 0.9	0.9990
17.5	72 ± 8	13.7 ± 0.3	0.9983
35	96 ± 8	9.1 ± 0.3	0.9963
70	108 ± 4	5.5 ± 0.1	0.9984
140	234 ± 8	3.4 ± 0.1	0.9985

investigated systems. From the fits, G and η have been determined as adjustable parameters. The values of the surface shear elasticity, E_{sh}, and viscosity, η_{sh}, are determined from G and η as follows:[4,44]

$$E_{sh} = g_f G, \qquad \eta_{sh} = g_f \eta \tag{4}$$

$$g_f \equiv \frac{1}{4\pi}\left(\frac{1}{R_1^2} - \frac{1}{R_2^2}\right) \tag{5}$$

g_f is a geometric factor; R_1 = 2.81 cm and R_2 = 3.00 cm are the inner and outer radii of the experimental ring-shaped interfacial domain, which is subjected to shearing (Figure 1). With these parameter values, eq 5 gives g_f = 12.36 rad/m^2. The advantage from using a relatively narrow gap, ΔR = 0.19 cm, is that eq 5 is applicable to systems of both linear and nonlinear rheological response. If the ratio $\Delta R/R_1$ is not small and the system exhibits a

dx.doi.org/10.1021/la205113w | Langmuir 2012, 28, 4168–4177

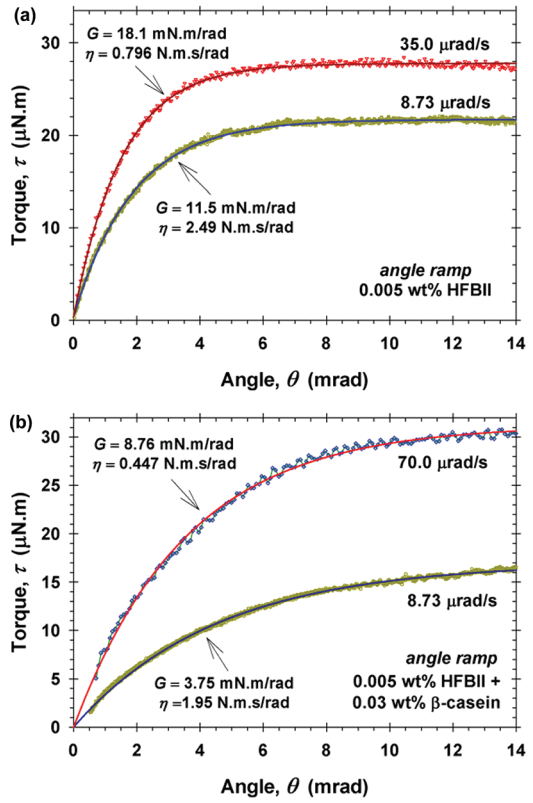

Figure 7. Examples for fits (the solid lines) of experimental data for torque τ vs angle θ with the Maxwell model. (a) 0.005 wt % HFBII; (b) 0.005 wt % HFBII + 0.03 wt % β-casein. The values of the angular velocity $\dot{\theta}$, and of G and η determined from the fits are shown in the figure for the respective curves.

nonlinear response (e.g., shear thinning), then g_f becomes dependent also on the layer's specific rheological properties and the simple eq 5 is not applicable. For narrow gaps, the meniscus in the gap might not be perfectly flat, which would result in larger effective ΔR and g_f. We carried out test measurements at ΔR = 0.10 and 0.19 cm, which gave identical results, so that the effect of meniscus seems to be inessential.

The results for E_{sh}, and η_{sh}, are given in Table 1. E_{sh} varies in the range from 50 to 250 mN/m. These values are large as compared to those measured for other proteins. For example, $E_{sh} \leq 38.2$ mN/m was measured for β-lactoglobulin.[45] The errors of E_{sh} and η_{sh} in Table 1 reflect the reproducibility of the experiment, rather than the accuracy of the separate measurement. If these errors are determined from a separate fit (Figure 7), then their values are smaller than those in Table 1.

4.2. Comparison with the Herschel–Bulkley Law. In Table 1, the surface shear viscosity, η_{sh}, systematically decreases with the rise of the shear rate $\dot{\theta}$ (shear thinning). As seen in Figure 8a, the data for η_{sh} obey the Herschel–Bulkley law:[46]

$$\tau_{sh} = K\dot{\theta}^n = \eta_{sh}\dot{\theta} \Rightarrow \eta_{sh} = K\dot{\theta}^{n-1} \quad (6)$$

In eq 6, $\tau_{sh} \equiv g_f\tau$ is the shear stress; K is the consistency and n is the flow behavior index; $n < 1$ for shear thinning, whereas $n > 1$ for shear thickening. The values of K and n determined from the fits in Figure 8a are given in Table 2.

Figure 8b compares the values of the shear elasticity, E_{sh}, for HFBII adsorption layers without and with β-casein. At the lower $\dot{\theta}$, the elasticity is greater for the HFBII layers, whereas at

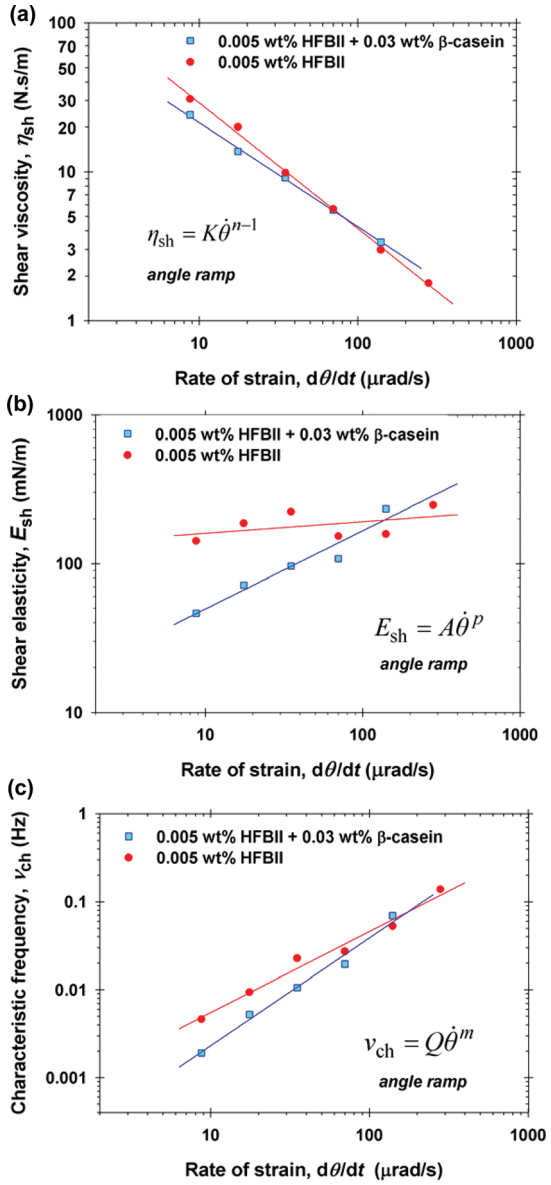

Figure 8. Plots of (a) the shear viscosity, η_{sh}, (b) the shear elasticity, E_{sh}, and (c) the characteristic frequency of the layer's rheological response, ν_{ch}, vs the rate of strain (angular velocity) $\dot{\theta}$ for 0.005 wt % HFBII with and without added β-casein. The lines are fits with the power functions shown in the figure.

Table 2. Parameters in Equations 6 and 7 Determined from Fits of the Data in Figure 8

solution	K N·s/m/(μrad/s)$^{1-n}$	n	m	p^a	Q (s^{m-1})
0.005 wt % HFBII	202 ± 18	0.16 ± 0.02	0.92 ± 0.07	0.08	663
0.005 wt % HFBII + 0.03 wt % β-casein	106 ± 6	0.30 ± 0.02	1.22 ± 0.09	0.52	139

[a] p is calculated from the relationship $p = m + n - 1$.

the higher $\dot{\theta}$, the elasticities for the two systems become comparable.

Figure 8c, shows the ratio $\nu_{ch} \equiv E_{sh}/\eta_{sh}$, which represents the characteristic frequency of the rheological response of the layer. ($t_{ch} \equiv 1/\nu_{ch}$ is the respective characteristic time.) In the framework of the Maxwell model (see Figure 6), an elastic body

dx.doi.org/10.1021/la205113w | Langmuir 2012, 28, 4168–4177

corresponds to $E_{sh} \rightarrow$ const, $\eta_{sh} \rightarrow \infty$, and consequently $\nu_{ch} = E_{sh}/\eta_{sh} \rightarrow 0$. In the other limit of a purely viscous fluid, we have $E_{sh} \rightarrow \infty$, $\eta_{sh} \rightarrow$ const, and consequently $\nu_{ch} \rightarrow \infty$. Hence, the characteristic frequency, varying in the range $0 < \nu_{ch} < \infty$ (0 = purely elastic body; ∞ = viscous fluid), provides a quantitative measure for the degree of softness (fluidity) of the investigated viscoelastic adsorption layers. In this respect, the increase of ν_{ch} with the rate of strain in Figure 8c indicates fluidization of the adsorption layer upon increasing of the shear rate. The addition of β-casein leads to more rigid layers at the lower rates of strain, but the difference becomes smaller at the higher rates of strain.

In analogy with eq 6, the data in Figures 8b and 8c can be also fitted with power functions:

$$E_{sh} = A\dot{\theta}^{p}, \qquad \nu_{ch} = Q\dot{\theta}^{m} \tag{7}$$

Because $\nu_{ch} \equiv E_{sh}/\eta_{sh}$, by definition we have $p = m + n - 1$. Parameter values determined from the fits are shown in Table 2. The fits in Figure 8b indicate the general tendency of the elasticity E_{sh} to increase with $\dot{\theta}$ in the investigated range of shear rates. The scattering of the E_{sh} values, especially for the layer from pure HFBII, is most probably due to the lower reproducibility of the respective measurements. The β-casein containing layers exhibit a faster tendency of fluidization with the rise of $\dot{\theta}$—compare the values of m in Table 2.

The variation of viscosity η_{sh} and elasticity E_{sh} with the shear rate $\dot{\theta}$ (see eqs 6 and 7 and Figure 8) is not in conflict with the use of the Maxwell model to fit the data (Figure 7). Indeed, in the angle-ramp regime $\dot{\theta}$ = const for each run, so that $\eta_{sh}(\dot{\theta})$ = const and $E_{sh}(\dot{\theta})$ = const for each experimental curve, like those in Figure 7.

4.3. Effect of β-Casein Concentration. Figure 9 shows the effect of β-casein concentration on E_{sh} and η_{sh} at shear rate

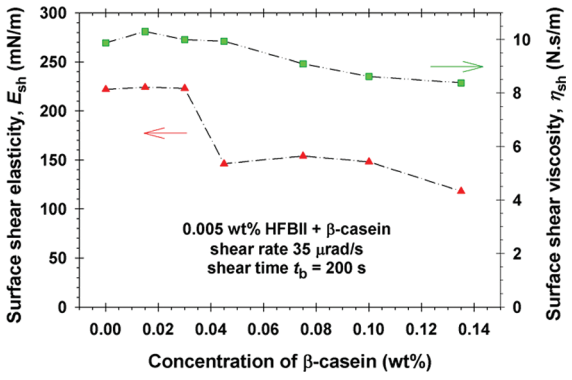

Figure 9. Effect of the addition of β-casein to 0.005 wt % HFBII solutions on the surface shear elasticity, E_{sh} and viscosity, η_{sh}, determined from the best fits of the experimental curves in Figure 5 for angle-ramp regime at a shear rate $\dot{\theta}$ = 35 μrad/s and shearing time t_b = 200 s.

$\dot{\theta}$ = 35 μrad/s and shear time t_b = 200 s. At β-casein concentrations $\leq$0.03 wt %, the values of both E_{sh} and η_{sh} are practically the same as for HFBII alone. At β-casein concentrations $\geq$0.045 wt %, E_{sh} becomes smaller with about 80 mN/m, but still remains relatively high, $\geq$120 mN/m.

This behavior indicates that an adsorption layer of HFBII is present at the air/water interface in all these experiments (Figure 9). The constancy of E_{sh} and η_{sh} at β-casein concentrations $\leq$0.03 wt % indicates negligible adsorption of β-casein at such low concentrations. Effects are detected at β-casein concentrations $\geq$0.045 wt %, at which both E_{sh} and η_{sh} begin to decrease.

We could hypothesize that the β-casein forms a second adsorption layer, below that of the hydrophobin. In addition, β-casein molecules may fill the voids in the hydrophobin monolayer thus affecting its rheological behavior. If the β-casein molecules were able to break the continuous HFBII network at the interface, this would lead to a dramatic drop of both E_{sh} and η_{sh}, but such a behavior is not observed in these experiments (Figure 9). The physical picture that emerges from the data analysis is that the adsorption from the mixed solutions of HFBII + β-casein leads to a spontaneous formation of an interfacial bilayer, which consists of a layer from the more hydrophobic HFBII that faces the air phase, and a layer of the more hydrophilic β-casein that faces the aqueous phase. It is remarkable that if the two proteins are let to spontaneously adsorb from the mixed solution, without external mechanical impacts, they separate in the formed interfacial bilayer.

If the described HFBII/β-casein bilayer is subjected to a more intensive or prolonged agitation, we may expect that the two protein components will begin to mix. Indication for such an effect is the value E_{sh} = 96.3 mN/m (at $\dot{\theta}$ = 35 μrad/s and 0.03 wt % β-casein) in Table 1; the respective value in Figure 9 is E_{sh} = 223 mN/m. This difference can be explained with the fact that the value E_{sh} = 96.3 mN/m is obtained at two times longer shearing time, t_b = 400 s (vs t_b = 200 s for the value in Figure 9). The experiments show that the agitation leads to a pronounced softening of the mixed HFBII + β-casein adsorption layers, which is observed also in oscillatory rheological measurements that will be reported in a subsequent paper.

5. RELAXATION REGIME: DATA INTERPRETATION

5.1. Modified Andrade's Cubic-Root Law. As described above, in our experiments after the angle-ramp (shearing), the torque τ relaxes at fixed rotation angle, $\theta = \theta_b$ for $t \geq t_b$. At relaxation, the τ-vs-t dependence is not exponential (as predicted by the Maxell model), but follows a cubic-root (Andrade's) law.[47−50] The data comply with the equation:

$$\tau \approx \tau_b\left[1 - \left(\frac{\Delta t}{t_{r1}}\right)^{1/3}\right], \qquad \Delta t \equiv t - t_b \tag{8}$$

where t_{r1} is a relaxation time and τ_b is a characteristic value of the torque. Note that the original Andrade's law refers to the time dependence of the *strain* of a solid subjected to load, whereas in our case eq 8 describes the relaxation of the *stress* upon solidification. This physical difference leads to different signs before the cubic root: In the original Andrade's law,[47−49] this sign is plus, whereas in eq 8 the sign is minus. For this reason, here eq 8, and its generalized form, eq 9, are termed modified Andrade's law.

The data in Figures 2−5 for τ vs t in relaxation regime ($t > t_b$) were fitted by eq 8, and the parameters τ_b and t_{r1} were determined from the fits. For example, in Figure 10a, the data from Figure 3 are plotted as τ/τ_b vs $(\Delta t)^{1/3}$ in accordance with eq 8. It is remarkable that the different relaxation curves in Figure 3 collapse on a single master curve (Figure 10a). The same happens with the data from Figure 4, which are plotted as τ/τ_b vs $(\Delta t)^{1/3}$ in Figure 10b. Each set of data is fitted with a straight line in accordance with eq 8. The determined parameters τ_b and t_{r1} are shown in Table 3. The values of the relaxation time t_{r1} practically coincide for a given system at different angular velocities of the shearing that has preceded the relaxation.

dx.doi.org/10.1021/la205113w | Langmuir 2012, 28, 4168−4177

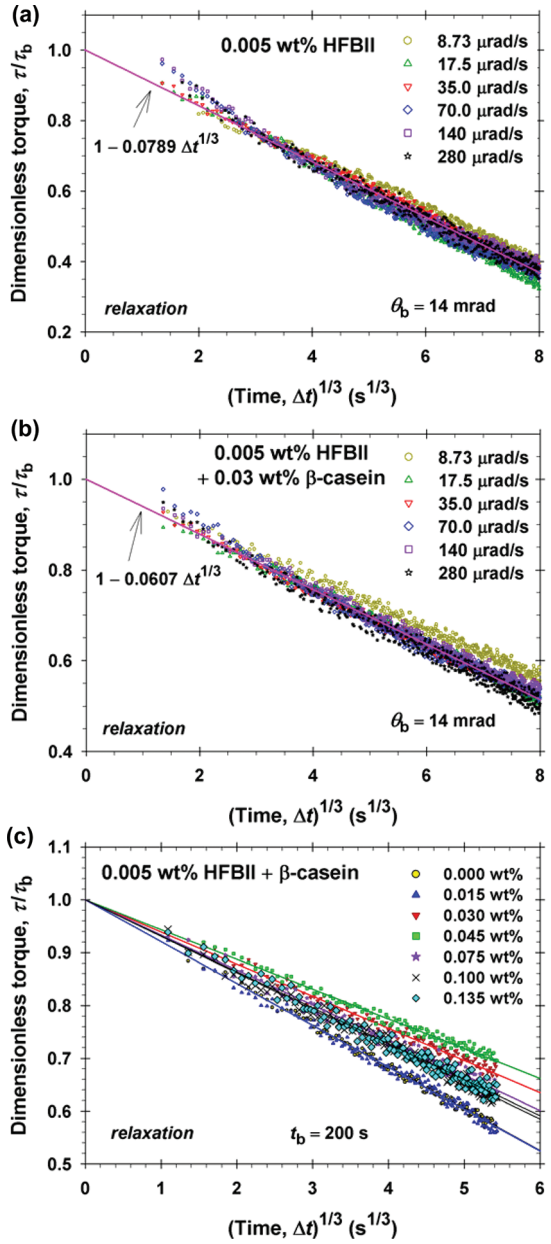

Figure 10. Relaxation regime ($t > t_b$): Plots of the dimensionless stress, τ/τ_b, vs cubic root of time, $(\Delta t)^{1/3}$, in accordance with eq 8. (a) Data from Figure 3 for 0.005 wt % HFBII and (b) from Figure 4 for 0.005 wt % HFBII +0.03 wt % β-casein, at different shear rates $\dot{\theta}$ of the preceding angle-ramp. (c) Data from Figure 5 for 0.005 wt % HFBII at $\theta = 35$ μrad/s, and at different concentrations of added β-casein given in the figure.

For this reason, the data sets in Figures 10a,b are fitted with a single straight line corresponding to the respective mean t_{r1} in Table 3.

It should be noted that the cubic-root (Andrade-type) relaxation does not begin immediately at $t = t_b$, when the shearing has been ceased. There is a transitional period of 5−10 s between the end of the angle-ramp regime and the relaxation in accordance with eq 8. In Figures 10a,b, the transitional period is manifested as deviations of the experimental points from the linear dependence at the smallest Δt. The points corresponding to the transitional regime have been excluded when drawing the linear regressions in Figure 10.

Table 3. Parameters of the Modified Andrade's Model (Equation 8) Determined from Fits of the Data in Relaxation Regime, $t > t_b$ (Figure 10a,b)

	0.005 wt % HFBII		0.005 wt % HFBII + 0.03 wt % β-casein	
$\dot{\theta}$ (μrad/s)	τ_b (μN·m)	t_{r1} (min)	τ_b (μN·m)	t_{r1} (min)
8.73	22.4	39.8	15.5	99.5[a]
17.5	28.2	30.0	19.7	75.7
35.0	29.2	35.2	29.6	72.9
70.0	32.2	30.6	27.5	74.7
140	31.0	34.5	35.4	79.9
280	34.4	33.6	24.7	68.9
mean:		33.9 ± 3.6	mean:	74.4 ± 4.0

[a]This value is not included when calculating the mean t_{r1}.

The mean values of the characteristic relaxation (solidification) time t_{r1} in Table 3 are about two times longer for the adsorption layers with β-casein, in comparison with those for HFBII alone. Hence, the data in Table 3 indicates that the addition of β-casein decelerates the solidification of the adsorption layer.

Table 4 shows the values of τ_b and t_{r1} for the stress relaxation after shearing for three different time intervals, t_b = 200, 400, and 800 s, at the same shear rate $\dot{\theta} = 35$ μrad/s; see Figure 2. The results indicate that in the considered case τ_b and t_{r1} are insensitive to t_b.

Table 4. Parameters of the Modified Andrade's Model (Equation 8) Determined from Fits of the Data in the Relaxation Regime ($t > t_b$) in Figure 2

t_b (s)	τ_b (μN·m)	t_{r1} (min)
200	30.3	33.8
400	29.2	35.2
800	29.6	32.2
mean:	29.7 ± 0.6	33.7 ± 1.5

Figure 10c shows plots of τ/τ_b vs $(\Delta t)^{1/3}$ at different concentrations of β-casein at the same $\dot{\theta} = 35$ μrad/s. For each separate β-casein concentration, the data comply very well with a linear dependence. The slopes of the lines are different for different β-casein concentrations. The determined values of the parameters τ_b and t_{r1} are given in Table 5. The relaxation time t_{r1} exhibits a maximum at an intermediate β-casein concentration.

Table 5. Parameters of the Linear Fits of the Data in Figure 10c for 0.005 wt % HFBII at Different Concentrations of Added β-Casein

β-casein (wt %)	τ_b (μN·m)	t_{r1} (min)
0.000	30.3	33.8
0.015	24.9	33.6
0.030	27.5	74.1
0.045	29.8	93.4
0.075	26.6	56.9
0.100	24.5	54.5
0.135	23.6	52.8

5.2. Long-Time Relaxation. The limiting transition $\Delta t \rightarrow \infty$ in eq 8 yields $\tau \rightarrow -\infty$, which is physically meaningless. This fact indicates that eq 8 represents a short-time asymptotics of a more general expression describing the whole relaxation

dx.doi.org/10.1021/la205113w | Langmuir 2012, 28, 4168−4177

process. To find it, we carried our experiments at much longer times; see Figures 11 and A1 (the latter is in Appendix A of the

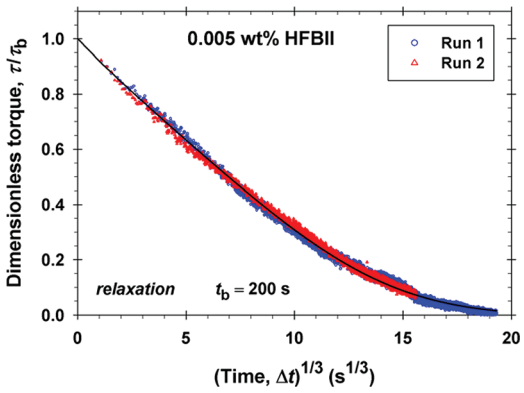

Figure 11. Plot of the dimensionless stress, τ/τ_b, vs cubic root of time, $(\Delta t)^{1/3}$, for solutions of 0.005 wt % HFBII (two runs); $\Delta t \equiv t - t_b$. The data are for the adsorption-layer relaxation after a preceding angle-ramp at shear rate $\dot{\theta}$ = 35 μrad/s for t_b = 200 s. The solid line is the best fit with eq 9.

Supporting Information). We tried to fit the data with different expressions, which give eq 8 as a short-time asymptotics (for $\Delta t \to 0$). The following relaxation law provides the best agreement with the experiment (see Figure 11):

$$\tau = \tau_b \exp\left[-\left(\frac{\Delta t}{t_{r1}}\right)^{1/3} - \frac{\Delta t}{t_{r2}}\right] \quad (9)$$

The parameter values determined from the fit are τ_b = 24.5 N·m; t_{r1} = 29.8 min, and t_{r2} = 47.5 min for adsorption monolayers at the surface of a 0.005 wt % HFBII solution. For sufficiently small Δt, the last term in the brackets in eq 9 is negligible and the exponent can be expanded in series to yield eq 8. The linear portion of the curve in Figure 11 at small Δt corresponds to the asymptotic eq 8 and to the experimental time intervals in Figure 10.

Equation 9 can be considered as a modified form of Andrade's law,[47] which was originally introduced to describe the creep of metals. The argument of the exponent in eq 8 corresponds (by magnitude) to one of the mathematical forms of the Andrade's law, which is obeyed by various materials with viscoelastic behavior; see, e.g., eq 2 in ref 51; eq 10 in ref 50; eq 3 in ref 52, and eq 11 in ref 53. In our case, eq 9 characterizes the relaxation of the stresses in a protein adsorption layer (after a preceding shearing) with two characteristic relaxation times: t_{r1} and t_{r2}.

6. CONCLUSIONS

The present article is the first study, in which the surface shear rheology of hydrophobin adsorption layers at the air/water interface is investigated in angle-ramp/relaxation regime and the obtained data are interpreted in the framework of a rheological model. In preceding studies,[7−9] the phenomenological storage and loss moduli, G' and G'', have been determined using rotational rheometer in oscillatory regime. The next step, viz. the determination of the true elasticity and viscosity of the viscoelastic surface layer, demands the use of an adequate rheological model. The main advantage of the angle-ramp regime is that it allows one to identify the rheological model, which quantitatively describes the behavior of the system. The obtained data at fixed shear rate, $\dot{\theta}$, are in excellent agreement with the Maxwell model (Figure 7). This enabled us to determine the surface shear elasticity and viscosity, E_{sh} and η_{sh} (Table 1). Furthermore, the dependence of η_{sh} on $\dot{\theta}$ obeys the Herschel−Bulkley law; see eq 6 and Figure 8a. A similar power law is obeyed by the characteristic frequency of rheological response: $\nu_{ch} = Q\dot{\theta}^m$. The latter quantity, which varies in the range $0 < \nu_{ch} < \infty$ (0 = purely elastic body; ∞ = viscous fluid), provides a quantitative measure for the degree of softness (fluidity) of the viscoelastic adsorption layers. The increase of ν_{ch} with the rise of $\dot{\theta}$ in Figure 8c indicates an increasing fluidization (softening) with the increase of $\dot{\theta}$. The addition of β-casein leads to more rigid adsorption layers, which exhibit a tendency of faster fluidization with the rise of $\dot{\theta}$ (Figure 8b). In other words, the softness/rigidity of different viscoelastic adsorption layers can be compared by putting together the respective $\nu_{ch}(\dot{\theta})$ dependences and values of the parameters Q and m.

Another novelty in the present study is that in relaxation regime, the HFBII adsorption layers obey a modified Andrade's law, eq 9, with two relaxation times, t_{r1} and t_{r2}, and a characteristic stress τ_b; see Figure 11. At shorter times, the relaxation curves obey a cubic-root asymptotics given by eq 8. The fits of the data give t_{r1} and τ_b; see Tables 3−5. For HFBII adsorption layers without additives, the relaxation time t_{r1} is independent of the rate and time of shearing of the preceding angle-ramp stage; see Tables 3 and 4. The data for HFBII solutions + β-casein, and especially the high E_{sh} values, indicate the formation of an interfacial bilayer, which consists of a layer from the more hydrophobic HFBII facing the air phase and a layer of the more hydrophilic β-casein that faces the water phase.

Thus, it turns out that the data for τ vs t comply with the Maxwell model (eq 2) in angle-ramp regime (section 4.1), but they follow the modified Andrade's low (eq 9) in relaxation regime (section 5). This difference can be explained with the different processes that occur in the viscoelastic adsorption layer in these two regimes: breakage and restoration of intermolecular bonds (at angle-ramp), and solidification of the adsorption layer (at relaxation).

■ ASSOCIATED CONTENT

Supporting Information

Appendix A: additional results. This material is available free of charge via the Internet at http://pubs.acs.org.

■ AUTHOR INFORMATION

Corresponding Author

*Telephone: (+359) 2-8161262. Fax: (+359) 2-9625643. E-mail: pk@lcpe.uni-sofia.bg.

Notes

The authors declare no competing financial interest.

■ ACKNOWLEDGMENTS

The authors gratefully acknowledge the support from Unilever Research and from the National Science Fund of Bulgaria, grant No. DO-02-121/2009. The authors are grateful to Ms. Mariana Paraskova for her assistance in figure preparation.

■ REFERENCES

(1) Graham, D. E.; Phillips, M. C. Proteins at Liquid Interfaces. V. Shear Properties. *J. Colloid Interface Sci.* **1980**, *76*, 240−250.

(2) Dickinson, E.; Murray, B. S.; Stainsby, G. Time-dependent surface viscosity of adsorbed films of casein + gelatin at the oil-water interface. *J. Colloid Interface Sci.* **1985**, *106*, 259−262.
(3) Langevin, D. Influence of interfacial rheology on foam and emulsion properties. *Adv. Colloid Interface Sci.* **2000**, *88*, 209−222.
(4) Borbas, R.; Murray, B. S.; Kiss, E. Interfacial shear rheological behavior of proteins in three-phase partitioning systems. *Colloids Surf., A* **2003**, *213*, 93−103.
(5) Freer, E. M.; Yim, K. S.; Fuller, G. G.; Radke, C. J. Shear and dilatational relaxation mechanisms of globular and flexible proteins at the hexadecane/water interface. *Langmuir* **2004**, *20*, 10159−10167.
(6) Reger, M.; Sekine, T.; Okamoto, T.; Hoffmann, H. Unique emulsions based on biotechnically produced hydrophobins. *Soft Matter* **2011**, *7*, 8248−8257.
(7) Cox, A. R.; Cagnol, F.; Russell, A. B.; Izzard, M. J. Surface properties of class II hydrophobins from *Trichoderma reesei* and influence on bubble stability. *Langmuir* **2007**, *23*, 7995−8002.
(8) Cox, A. R.; Aldred, D. L.; Russell, A. B. Exceptional stability of food foams using class II hydrophobin HFBII. *Food Hydrocolloids* **2009**, *23*, 366−376.
(9) Blijdenstein, T. B. J.; de Groot, P. W. N.; Stoyanov, S. D. On the link between foam coarsening and surface rheology: why hydrophobins are so different. *Soft Matter* **2010**, *6*, 1799−1808.
(10) Panaiotov, I.; Dimitrov, D. S.; Ter-Minassian-Saraga, L. Dynamics of insoluble monolayers. II. Viscoelastic behavior and Marangoni effect for mixed protein phospholipid films. *J. Colloid Interface Sci.* **1979**, *72*, 49−53.
(11) Vassilev, P. M.; Taneva, S.; Panaiotov, I.; Georgiev, G. Dilatational viscoelastic properties of tubulin and mixed tubulin-lipid monolayers. *J. Colloid Interface Sci.* **1981**, *84*, 169−174.
(12) Krägel, J.; Wüstneck, R.; Clark, D.; Wilde, P.; Miller, R. Dynamic surface tension and surface shear rheology studies of mixed β-lactoglobulin/Tween 20 systems. *Colloids Surf., A* **1995**, *98*, 127−135.
(13) Krägel, J.; Wüstneck, R.; Husband, F.; Wilde, P. J.; Makievski, A. V.; Grigoriev, D. O.; Li, J. B. Properties of mixed protein/surfactant adsorption layers. *Colloids Surf., B* **1999**, *12*, 399−407.
(14) Roth, S.; Murray, B. S.; Dickinson, E. Interfacial shear rheology of aged and heat-treated β-lactoglobulin films: displacement by nonionic surfactant. *J. Agric. Food Chem.* **2000**, *48*, 1491−1497.
(15) Gunning, P. A.; Mackie, A. R.; Gunning, P; Woodward, N. C.; Wilde, P. J.; Morris, V. J. Effect of surfactant type on surfactant-protein interactions at the air-water interface. *Biomacromolecules* **2004**, *5*, 984−991.
(16) Krägel, J.; Derkatch, S. R.; Miller, R. Interfacial shear rheology of protein-surfactant layers. *Adv. Colloid Interface Sci.* **2008**, *144*, 38−53.
(17) Murray, B. S.; Dickinson, E. Interfacial rheology and the dynamic properties of adsorbed films of food proteins and surfactants. *Food Sci. Technool.* **1996**, *2*, 131−145.
(18) Miller, R.; Wüstneck, R.; Krägel, J.; Kretzschmar, G. Dilational and shear rheology of adsorption layers at liquid interfaces. *Colloids Surf., A* **1996**, *111*, 75−118.
(19) Dickinson, E. Milk protein interfacial layers and the relationship to emulsion stability and rheology. *Colloids Surf., B* **2001**, *20*, 197−210.
(20) Bos, M. A.; van Vliet, T. Interfacial rheological properties of adsorbed protein layers and surfactants: a review. *Adv. Colloid Interface Sci.* **2001**, *91*, 437−471.
(21) Krägel, J.; Derkatch, S. R. Interfacial shear rheology. *Curr. Opin. Colloid Interface Sci.* **2010**, *15*, 246−255.
(22) Miller, R.; Ferri, J. K.; Javadi, A.; Krägel, J.; Mucic, N.; Wüstneck, R. Rheology of interfacial layers. *Colloid Polym. Sci.* **2010**, *288*, 937−950.
(23) Basheva, E. S.; Kralchevsky, P. A.; Christov, N. C.; Danov, K. D.; Stoyanov, S. D.; Blijdenstein, T. B. J.; Kim, H.-J.; Pelan, E. G.; Lips, A. Unique properties of bubbles and foam films stabilized by HFBII hydrophobin. *Langmuir* **2011**, *27*, 2382−2392.
(24) Basheva, E. S.; Kralchevsky, P. A.; Danov, K. D.; Stoyanov, S. D.; Blijdenstein, T. B. J.; Pelan, E. G.; Lips, A. Self-assembled bilayers from the protein HFBII hydrophobin: nature of the adhesion energy. *Langmuir* **2011**, *27*, 4481−4488.
(25) Linder, M. B.; Szilvay, G. R.; Nakari-Setälä, T.; Penttila, M. Hydrophobins: the protein-amphiphiles of filamentous fungi. *FEMS Microbiol. Rev.* **2005**, *29*, 877−896.
(26) Sunde, M.; Kwan, A. H. Y.; Templeton, M. D.; Beever, R. E.; Mackay, J. P. Structural analysis of hydrophobins. *Micron* **2008**, *39*, 773−784.
(27) Linder, M. B. Hydrophobins: proteins that self assemble at interfaces. *Curr. Opin. Colloid Interface Sci.* **2009**, *14*, 356−363.
(28) Zhang, X. L.; Penfold, J.; Thomas, R. K.; Tucker, I. M.; Petkov, J. T.; Bent, J.; Cox, A. Adsorption behavior of hydrophobin and hydrophobin/surfactant mixtures at the solid−solution interface. *Langmuir* **2011**, *27*, 10464−10474.
(29) Zhang, X. L.; Penfold, J.; Thomas, R. K.; Tucker, I. M.; Petkov, J. T.; Bent, J.; Cox, A.; Grillo, I. Self-assembly of hydrophobin and hydrophobin/surfactant mixtures in aqueous solution. *Langmuir* **2011**, *27*, 10514−10522.
(30) Zhang, X. L.; Penfold, J.; Thomas, R. K.; Tucker, I. M.; Petkov, J. T.; Bent, J.; Cox, A.; Campbell, R. A. Adsorption behavior of hydrophobin and hydrophobin/surfactant mixtures at the air−water interface. *Langmuir* **2011**, *27*, 11316−11323.
(31) Reger, M.; Sekine, T.; Okamoto, T.; Watanabe, K.; Hoffmann, H. Pickering emulsions stabilized by novel clay−hydrophobin synergism. *Soft Matter* **2011**, *7*, 11021−11030.
(32) Aumaitre, E.; Vella, D.; Cicuta, P. On the measurement of the surface pressure in Langmuir films with finite shear elasticity. *Soft Matter* **2011**, *7*, 2530−2537.
(33) Aumaitre, E.; Wongsuwarn, S.; Rossetti, D.; Hedges, N. D.; Cox, A. R.; Vella, D.; Cicuta, P. A viscoelastic regime in dilute hydrophobin monolayers. *Soft Matter* **2012**, *8*, 1175−1183.
(34) Panaiotov, I.; Ivanova, Tz.; Proust, J.; Boury, F.; Denizot, B.; Keough, K.; Taneva, S. Effect of hydrophobic protein SP-C on structure and dilatational properties of the model monolayers of pulmonary surfactant. *Colloids Surf., B* **1996**, *6*, 243−260.
(35) Hambardzumyan, A.; Aguié-Béghin, V.; Panaiotov, I.; Douillard, R. Effect of frequency and temperature on rheological properties of β-casein adsorption layers. *Langmuir* **2003**, *19*, 72−78.
(36) Ivanova, Tz.; Minkov, I.; Panaiotov, I.; Saulnier, P.; Proust, J. E. Dilatational properties and morphology of surface films spread from clinically used lung surfactants. *Colloid Polym. Sci.* **2004**, *282*, 1258−1267.
(37) Bantchev, G. B.; Schwartz, D. K. Surface shear rheology of β-casein layers at the air/solution interface: formation of a two-dimensional physical gel. *Langmuir* **2003**, *19*, 2673−2682.
(38) Lee, M. H.; Reich, D. H.; Stebe, K. J.; Leheny, R. L. Combined passive and active microrheology study of protein-layer formation at an air-water interface. *Langmuir* **2010**, *26*, 2650−2658.
(39) Erni, P.; Fischer, P.; Windhab, E. J.; Kusnezov, V.; Stettin, H.; Läuger, J. Stress- and strain-controlled measurements of the interfacial shear viscosity and viscoelasticity at liquid/liquid and gas/liquid interfaces. *Rev. Sci. Instrum.* **2003**, *74*, 4916−4924.
(40) Paananen, A.; Vuorimaa, E.; Torkkeli, M.; Penttilä, M.; Kauranen, M.; Ikkala, O.; Lemmetyinen, H.; Serimaa, R.; Linder, M. B. Structural hierarchy in molecular films of two class II hydrophobins. *Biochemistry* **2003**, *42*, 5253−5258.
(41) Szilvay, G. R.; Paananen, A.; Laurikainen, K.; Vuorimaa, E.; Lemmetyinen, H.; Peltonen, J.; Linder, M. B. Self-assembled hydrophobin protein films at the air-water interface: structural analysis and molecular engineering. *Biochemistry* **2007**, *46*, 2345−2354.
(42) Torkkeli, M.; Serimaa, R.; Ikkala, O.; Linder, M. Aggregation and self-assembly of hydrophobins from *Trichoderma reesei*: low-resolution structural models. *Biophys. J.* **2002**, *83*, 2240−2247.
(43) Askolin, S.; Linder, M.; Scholtmeijer, K.; Tenkanen, M.; Penttilä, M.; de Vocht, M. L.; Wösten, H. A. B. Interaction and comparison of a class I hydrophobin from Schizophyllum commune and class II hydrophobins from Trichoderma reesei. *Biomacromolecules* **2006**, *7*, 1295−1301.

(44) Landau, L. D.; Lifshitz, E. M. *Fluid Mechanics (Course of Theoretical Physics, Vol. 6)*, 2nd ed.; Butterworth-Heinemann: Oxford, UK, 1987.
(45) Petkov, J.; Gurkov, T.; Campbell, B.; Borwankar, R. Dilatational and shear elasticity of gel-like protein layers on air/water interface. *Langmuir* **2000**, *16*, 3703−3711.
(46) Herschel, W. H.; Bulkley, R. Konsistenzmessungen von Gummi-Benzollösungen. *Kolloid Z.* **1926**, *39*, 291−300 doi: 10.1007/BF01432034.
(47) Andrade, E. N.; da, C. On the viscous flow in metals, and allied phenomena. *Proc. R. Soc. A-Math. Phys. Eng. Sci.* **1910**, *84*, 1−12.
(48) Andrade, E. N.; da, C. The flow in metals under large constant stresses. *Proc. R. Soc. A-Math. Phys. Eng. Sci.* **1914**, *90*, 329−342.
(49) Andrade, E. N.; da, C.; Jolliffe, K. H. The flow of polycrystalline metals under simple shear. II. *Proc. R. Soc. A-Math. Phys. Eng. Sci.* **1960**, *254*, 291−316.
(50) Plazek, D. J. Dynamic mechanical and creep properties of a 23% cellulose nitrate solution; Andrade creep in polymeric systems. *J. Colloid Sci.* **1960**, *15*, 50−75.
(51) Glen, J. W. The creep of polycrystalline ice. *Proc. R. Soc. A-Math. Phys. Eng. Sci.* **1955**, *228*, 519−538.
(52) Plazek, D. J.; Dannhauser, W.; Ferry, J. D. Viscoelastic dispersion of polydimethyl siloxane in the rubberlike plateau zone. *J. Colloid Sci.* **1961**, *16*, 101−126.
(53) Vacin, O. J.; Stastna, J.; Zanzotto, L. Creep compliance of polymer-modified asphalt, asphalt mastic, and hot-mix asphalt. *Transp. Res. Record* **2003**, *1829*, 33−38 doi: 10.1007/BF01432034.